Thermal infrared geostationary satellite sensor data application for prediction and monitoring earthquake in Algeria

Abdelatif Hassini*

Département de Maintenance en Instrumentation,
Institut de Maintenance et Sécurité Industrielle,
Université d'Oran 2 Mohamed Ben Ahmed,
BP 1524, El M'Nouar, Oran, Algeria
Email: hassini.abdelatif@univ-oran.dz
*Corresponding author

Ahmed Hafid Belbachir

Laboratoire d'Analyse et d'Application des Rayonnements,
Faculté de Physique,
Université USTOMB,
BP 1505, El M'Nouar, Bir El Djir, Oran, Algeria
Email: ahmedhafidbelbachir@gmail.com

Abstract: The modern operational space-borne optical sensors in the thermal infrared spectrum allow monitoring of the Earth's thermal field for detection of pre-earthquake thermal infrared (TIR) anomaly in land surface temperature in and around epicentral areas. Based on the concept that stress in rocks in tectonically-active regions may be manifested as temperature variation through energy transformation process, remote sensing-based thermal technique has been employed recently. A new method called Active Earthquake Prediction Algorithm (AEPA) using an acquired thermal infrared time series satellite sensors datasets is developed and applied in this research. This approach can depict some anomalous increases in surface temperature that occur before an earthquake. Some past earthquakes in Algeria were analysed for studying successively before, during and after, and spatially close to, a significant earthquake continuous satellite data recording. The study was successful in detecting pre-earthquake thermal anomalies prior to all these natural disasters.

Keywords: earthquake; remote sensing; satellite sensor; surface temperature; AEPA algorithm; prediction; thermal anomalies information technology management; Algeria.

Reference to this paper should be made as follows: Hassini, A. and Belbachir, A.H. (2016) 'Thermal infrared geostationary satellite sensor data application for prediction and monitoring earthquake in Algeria', *Int. J. Information Technology and Management*, Vol. 15, No. 4, pp.293–312.

Biographical notes: Abdelatif Hassini received his HDR in Physics from the University of Oran, Algeria. He is currently a Lecturer and Assistant Professor in Applied Physics and Sensors at the University of Oran 2 Mohamed Ben Ahmed, Algeria. He is a member of Laboratory of Analysis and Application of Radiations (LAAR), Faculty of Physics, University of Sciences and Technology USTOMB. His research focuses on the use of the remote sensing data to extract thematic products used in the environment.

Ahmed Hafid Belbachir received his PhD in Nuclear Physics from the University of Michigan, USA. He is currently a Lecturer and Professor in Atomic Physics at University USTOMB, Algeria, and Head of Laboratory LAAR. His research focuses on physics in radiation detection.

This paper is a revised and expanded version of a paper entitled 'Thermal method of remote sensing for prediction and monitoring earthquake' presented at The 1st IEEE International Conference on Information and Communication Technologies for Disaster Management (ICT-DM'2014), Algeirs, Algeria, 24–25 March 2014.

1 Introduction

Earthquakes, floods, fires, volcanic eruptions, and mudslides are all natural disasters often unavoidable, but their effects may be limited by using robust techniques. A wide range of satellite methods is applied now in seismology. The first applications of satellite data for earthquake exploration were initiated in the 1970s when active faults were mapped on satellite images. It was a pure and simple extrapolation of airphoto geological space interpretation methods (Tronin, 2010).

The Earth's radiating temperature is at its lowest temperature of about 273°K (Ahrens and Henson, 2014). The distribution of full radiative energy at the two temperatures is shown in Figure 1. The sun emission covers the UV, visible and infrared radiations. The emission from the Earth, which is determined by the surface temperature, is primarily in the thermal infrared (TIR) spectral field. This parameter can be used to depict temperature anomalies which can be caused by pre-earthquake activities. The direct solar radiation at 10 μm is still several orders of magnitude greater than the thermal emission. However, the Earth's surface diffuses solar radiation and also has a high emittance (low reflectance) at 10 μm. Thus, it is found that at 10 μm, reflected solar radiation is only a small component of the emission, and it can be neglected. The converse is also true; emitted infrared radiation can be neglected when measuring reflected solar radiation at visible wavelengths (Platt, 1991).

The Mediterranean region is seismically active due to the northward convergence (4–10 mm/yr) of the African plate with respect to the Eurasian plate along a complex plate boundary. In this region there is a written record, several centuries long, documenting pre-instrumental seismicity (pre-20th century). Earthquakes had historically caused widespread damage across central and southern Greece, Cyprus, Sicily, Crete, the Nile Delta, Northern Libya, the Atlas Mountains of North Africa and the Iberian Peninsula.

Algeria is a nation plagued by earthquakes; there are typically five of moderately severe earthquakes every year. The 1980 M7.3 El Asnam earthquake was one of the Africa's largest and most destructive earthquakes within the 20th century. The most severe earthquake to occur in recent ten years was the Boumerdès earthquake of May 21, 2003 (M = 6.8), in which 2,266 lives were lost, 10,261 people injured and 200,000 left homeless as a result of the earthquake. Reports indicate more than 1,243 buildings were completely or partially destroyed. Infrastructure was predictably damaged in Algiers, Boumerdès, Réghaïa and Thénia (Curtis and Edwards, 2004).

The whole of Algeria is now routinely monitored by the 'Active Earthquake Prediction Algorithm' or AEPA method developed through this paper. A method in which TIR data from Spanning Enhanced in Visible and InfraRed Imager-METEOSAT Second Generation (SEVIRI-MSG) satellite sensor identifies anomalous increases in surface temperature that occurs, before an earthquake. The surface temperature may typically increase by 2°K to 6°K anywhere between several days and a month in advance of an earthquake. Data from the project, which was originally scheduled to last for ten years and a half, are daily acquired via a simple installed station and with some parts realised in the Laboratory of Analysis and Application of Radiations (LAAR) situated in the University of Sciences and Technology of Oran (North West of Algeria) (Hassini and Belbachir, 2013). The main objective of our station is to predict some natural hazards (like forest fires, earthquake, inundation…, etc.) so as to facilitate disaster reduction.

Figure 1 Distribution of radiance emitted from a full (blackbody) radiation at temperatures corresponding to the sun and the Earth

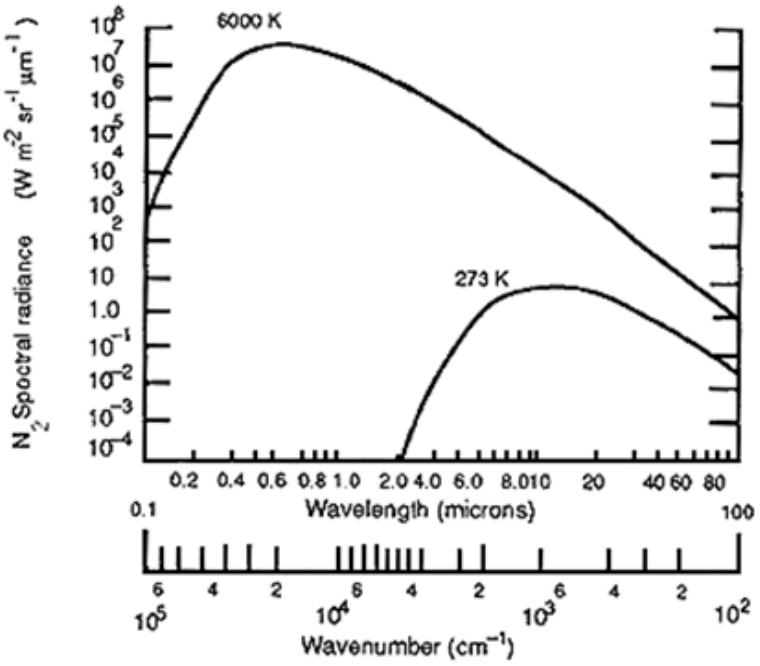

The AEPA method is helping to reduce death rate and financial impact of earthquakes in Algeria and other nations observed by satellite instruments. It offers an inexpensive and potentially more accurate alternative to other earthquake detection methods such as the GPS method. The latter relies on measurements of the slight deformation of the Earth's crust that occurs before an earthquake because of the wide coverage and ready availability of data (Kerkmann, 2004; Choudhury, 2005). In this research work, the method is primarily applied to an earthquake event that happened in the north west of Algeria (Oran city) six years ago with a shock magnitude of 5.5 Ms. One person was killed by a rockfall and more than 30 people were injured there. Several houses were destroyed at Gambetta District. The earthquake was felt in other Algerian areas such as

Hassi Mameche in Mostaganem and Sidi Bel Abbes. It was equally felt abroad in Huercal-Overa, Lumbreras, Mazarron and Torrevieja in Spain (Hassini and Belbachir, 2014).

The rest of this paper is structured as follows. Section 2 describes exhaustive characteristics of satellite data and additional resources used and details the proposed AEPA algorithm to predict active earthquakes. Section 3 shows some obtained scientific results by using the proposed algorithm on two occurred earthquakes with some comments and discussions. Finally, we conclude this research.

2 Materials and methods

2.1 Detailed characteristics of MSG satellite

The new generation of METEOSAT satellites, known as MSG, is spin-stabilised and capable of greatly-enhanced Earth observations. The satellite's 12-channel SEVIRI imager observes the half full disk of the Earth (centred in Africa) with an unprecedented repeat cycle of 15 minutes in 12 spectral wavelength regions or channels. The MSG program covered a series of three identical satellites (MSG-1 lunched in 2003, MSG-2 lunched in 2007 and MSG3 lunched in 2011) which are expected to provide observations and services over at least 12 years. Each satellite has an expected seven-year lifetime. According to the original METEOSAT system, MSG is planned as a dual-satellite service where one additional satellite is available in orbit. Currently, MSG-3 is the principal operative satellite.

Table 1 Spectral channel characteristics of SEVIRI in terms of central, minimum and maximum wavelength and the main application areas of each channel

Channel no.	*Spectral band (μm)*	*Characteristics of spectral band (μm)*			*Main observational application*
		λ_{cen}	λ_{min}	λ_{max}	
1	VIS0.6	0.635	0.56	0.71	Surface, clouds, wind fields
2	VIS0.8	0.81	0.74	0.88	Surface, clouds, wind fields
3	NIR1.6	1.64	1.50	1.78	Surface, cloud phase
4	IR3.9	3.90	3.48	4.36	Surface, clouds, wind fields
5	WV6.2	6.25	5.35	7.15	Water vapour, high level clouds, atmospheric instability
6	WV7.3	7.35	6.85	7.85	Water vapour, atmospheric instability
7	IR8.7	8.70	8.30	9.1	Surface, clouds, atmospheric instability
8	IR9.7	9.66	9.38	9.94	Ozone
9	IR10.8	10.80	9.80	11.80	Surface, clouds, wind fields, atmospheric instability
10	IR12.0	12.00	11.00	13.00	Surface, clouds, atmospheric instability
11	IR13.4	13.40	12.40	14.40	Cirrus cloud height, atmospheric instability
12	HRV	Broadband (about 0.4 – 1.1 μm)			Surface, clouds

The primary mission of the second generation METEOSAT satellites is the continuous observation of the Earth's full disk with a multi-spectral imager. The high temporal resolution for full-disk imaging compared to polar satellites provides multi-spectral observations of rapidly-changing phenomena such as deep convection (Chmyrev et al., 2013; Ma et al., 2010). It also provides better retrieval of wind fields obtained from the tracking of clouds, water vapour, and ozone features. Table 1 shows the spectral channel characteristics of SEVIRI radiometer and their primary applications.

There are two main channels (IR3.9 and IR10.8) widely used for Earth surface temperature. The radiance emission peak for blackbody surfaces is around 4 μm (Wien's Displacement Law), and this corresponds with MSG channel IR3.9 and the ambient temperature of 290°K. The radiance peak is approximately at 10 μm (MSG channel IR10.8). Therefore, IR3.9 channel is more sensitive to changes in temperatures than other channels and picks up spot temperature anomalies caused by the slight deformation of the Earth's crust. Hence, it is mostly used in earthquake prediction.

2.2 Use of Satellite data and additional resources

In this research, we have used the TIR channel (IR3.9) for SEVIRI sensor, because of it high sensitivity to changes in terrestrial temperature and it saturation point (335°K) is higher than most of other satellite sensors. The data from this instrument are received and calibrated to determine the brightness temperature and then to undergo geometric correction (plate Carrée correction) using information on the atmospheric temperature and pressure. Each data is then geo-referenced and calibrated in order to produce a TIR map. Analysis of these maps is performed in order to identify surface temperature anomalies which may be indicative of future earthquake activity. From an anomaly's character, the time, location and magnitude of an earthquake may be predicted.

Some of in-situ data used in this research are obtained from the European Mediterranean Seismological Center (EMSC), which members are seismological institutes and observatories of the Euro-Med region, it hosted since 1992 by the LDG (Laboratoire de Détection et de Géophysique, France). Its main scientific activities are the real-time earthquake information (RTEI) services and the production of the Euro-Med Bulletin (Godey et al., 2006). EMSC offers several services in the field of rapid information on the European-Mediterranean seismicity and significant earthquakes worldwide:

- Source parameters (origin time, epicentre location, focal depth, magnitude).
- Phase pickings (station code, arrival times, phase type, amplitudes and periods). Some messages only contain a group of phase pickings without any associated location.
- Moment tensors solutions, focal mechanisms.
- Other data.

2.3 Satellite images from raw data to surface temperature

Finally, IR3.9 data acquired from the MSG-SEVIRI imagers are scaled radiances packaged in 10-bit words. The conversion of the raw data from the instruments to scaled

radiances is carried out in real-time in the header part of each received image. Secondly, we converted the ten-bit SEVIRI count values (0–1,023) of IR3.9 TIR channels into scene radiances, brightness temperatures, and eight-bit word counts (Hassini et al., 2009).

The first step is to convert raw counts to radiances with equation (1).

$$R = (C_T - I)/S \tag{1}$$

where R is radiance in mW/(m^2.sr.cm^{-1}) and C_r is the raw count value (from SEVIRI). The coefficients S and I are the 'scaling' slope and intercept, respectively, and appear in the header part of each acquired image. The units of S are counts / (mW / [m^2.sr.cm^{-1}]). Their values depend on channel and not on detector. For a given channel, we expect them to be constant all the time and identical for each aforementioned satellite.

To convert radiance to temperature, one first uses equation (2) (the inverse of the Planck function) to derive effective temperature:

$$T_{eff} = (c_2 \nu)/\ln(1 + [c_1 \nu^3]/R) \tag{2}$$

where T_{eff} is the effective temperature (in °K), 'ln' stands for natural logarithm, and R is for radiance. The coefficients c_1 and c_2 are the two radiation constants, given by:

$$c_1 = 1.191066\,10^{-5}\ \mathrm{mW}/(\mathrm{m}^2.\mathrm{sr}.\mathrm{cm}^{-4})$$

$$c_2 = 1.438833\,°\mathrm{K}/\mathrm{cm}^{-1}$$

The quantity ν is the central wave number of the channel. For a given channel it may vary slightly among detectors, and it will vary from instrument to instrument. To convert effective temperature T_{eff} to actual surface temperature T_s (°K), one uses equation (3):

$$T_s = \beta.T_{eff} + \alpha \tag{3}$$

where the constants α and β depend on channel, detector, and instrument. The use of T_{eff} accounts for the variation of the Planck function across the spectral passband of the channel. The differences between the values of T_s and T_{eff} increase with decreasing temperature. They are usually of the order of 0.1°K. In the worst case, near 180°K, they are approximately 0.3°K.

The 1 byte count value X_a is derived from the surface temperature with equation (4) and equation (5) (Bristor, 1975).

$$\text{For } 163°\mathrm{K} <= Ts <= 242°\mathrm{K},\ X_a = 418 - T. \tag{4}$$

$$\text{For } 242°\mathrm{K} <= Ts <= 330°\mathrm{K},\ X_a = 660 - 2T. \tag{5}$$

X_a values are on an eight-bit scale and range in value from 0 to 255, with high counts representative of low surface temperatures. Beyond the difference in precision, there is a fundamental difference between a raw SEVIRI count and X_a count in their units. The first one is scaled radiance, whereas the last one is temperature.

2.4 AEPA description

The main steps of the process of AEPA are as follows:

1 Identify isolated area of TIR increase. The surface temperature X_a may typically increase by 2 to 6°K or higher than the sounding area. This means a choice of a region of interest on the surface temperature image and a calculation of the absolute value of the difference in a central pixel and the eight neighbouring ones.

2 Track the direction of the development and movement of the surface temperature increase area. This means a classification of all the temperature anomaly pixels on each surface temperature image according to the distribution of the histogram 2D.

3 Identify the surface temperature increase phenomenon as a precursor of earthquake by taking into consideration the effects of weather, topography, geomorphology, geotectonic and present tectonics stress field. This means the elimination of all non-anomalous background pixels such as those of cloud, water, and sand, followed by projection latitude, longitude, and altitude of each image pixel and its evolution. Then, a comparison is made between the result and its relationship and the large-scale structure of the Earth's crust and historical seismicity of the region of interest.

4 Provide a three-element prediction (earthquake time, location and magnitude) by considering the distribution of active fractures and seismic belts.

Prediction estimates are based upon:

- Time: after the identification of a surface TIR anomaly of a certain size and condition, earthquakes tend to occur probably within 1–15 days.
- Location: the directional 'front' of the surface temperature increase area is used to identify the epicentre of an earthquake:
- Magnitude:
  1 surface temperature increase area larger than 12 105 Km^2~Ms 7
  2 surface temperature increase area larger than 4 105 Km^2~Ms 6
  3 surface temperature increase area larger than 2 105 Km^2~Ms 5
  4 surface temperature increase area larger than 0.8 105 Km^2~Ms 4
  5 i.e., the larger the area the larger the main shock.

Surface temperature increases detected as precursors of earthquakes have been noted to possess the following characteristics:

1 The abnormal temperature increase area is identifiable. It usually demonstrates itself as an isolated body in the TIR image, and could be distinguished from other signals such as temperature anomalies caused by weather processes.

2 Our prediction practices prove that the tracking of surface temperature anomalous increases as earthquake precursors is universally valid.

3 The temperature of the anomalous area is typically 2°K to 6°K higher than that of its surroundings.

4 The larger the area of the surface temperature anomaly, the larger the magnitude of the future earthquake.

5 The dynamic evolution of the anomaly area and location may be monitored by satellite to predict the location of earthquake.

These steps are shown and summarised in the flow chart of Figure 2.

Figure 2 An overview of the steps in developing the AEPA algorithm

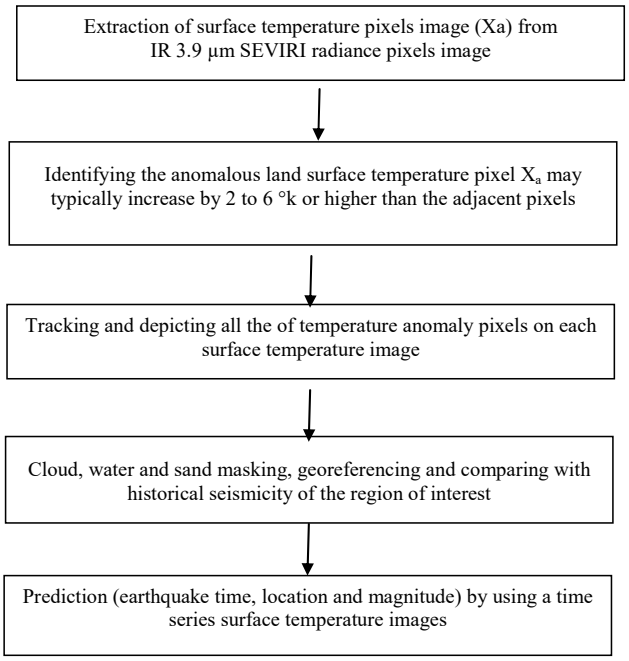

Note: The raw and processed data from this research are stored continuously and daily since October 27, 2007 from MSG-SEVIRI.

Based on our observations and experiments, we could suggest a preliminary model for the mechanism of the anomalous temperature increase as follows in Figure 3.

Some complexities which we met in this method can be cited as follows:

1 A difference in the time of appearance of the thermal IR anomalies has been observed in daytime and not nighttime, the IR3.9 channel records the reflected energy from the sun and Earth's radiant energy during the day and during the night it records the emitted energy from the earth only. This means that this channel has different responses during day and night.

2 Typical meteorological phenomena such as cloud appearance in processed images presents a big inconvenience which is that satellite thermal sensor signal cannot penetrate thick clouds to retrieve surface temperature. This occurs because continuous temperature data cannot be retrieved and some thermal anomaly information is previously lost.

3 Some false temperature anomalies detections were persistently observed in some deserts and sparsely vegetated land surfaces and in some cases earthquakes of small magnitude were not detected at all and most of these were mainly caused by the algorithm tests.

The approximate computational complexity for the AEPA algorithm depends on the complexity for calculation anomalies on surface temperature pixels. The simple way to think of this, is that if we extracted $m \times n$ surface temperature anomaly pixels from each an $M \times N$ (grayscale) half full disk MSG image, each pixel would need O(mn) computations, therefore, the 2D full disk MSG surface temperature extraction image would have an approximate computational complexity of O($MNmn$).

Figure 3 A preliminary model for the mechanism of the anomalous temperature increase, based in AEPA

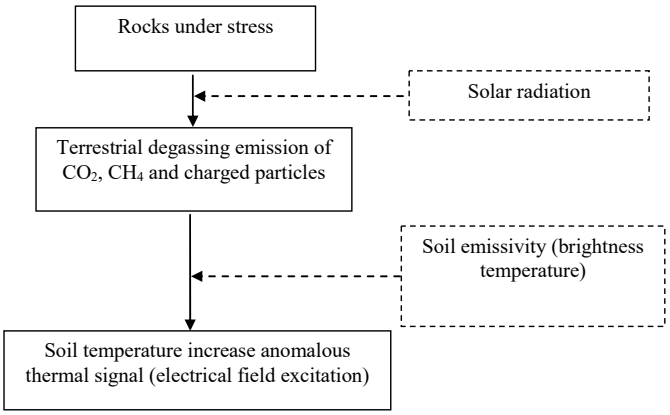

3 Results and discussions

Based on the thermal anomalous temperature increase, depicted by using AEPA method, we predicted that there would be an earthquake of magnitude 5 to 6 (Mw) in the north-western sea areas of Oran town (in North West of Algeria) on June 6th, 2008. The predicted time window was from June 1st to June 10th, 2008. As expected, there was an earthquake of magnitude 5.5 (Mw) on June 6th, 2008 at 20:02 UTC. The epicentre was located at 35.883N, 0.658W. The predicted location was in the sea, which is 20 Km away from the Bousfer Beach. In early June, 2008, an anomalous surface temperature increase appeared in the 3.9 μm thermal infrared band of SEVIRI-MSG2 imagery in the north west of Algeria. Figure 4 presents a scenario covering this event illustrated from the European-Mediterranean Seismological Centre (EMSC) (EMSC, 2015; Godey et al., 2013).

Figure 5 shows time series composite SEVIRI raw IR3.9 channels acquired from 4th to 7th June 2008 at 12:00 UTC (before and after the earthquake) with the corresponding histogram. Figure 6 provides time series of the surface temperature composite maps by using AEPA algorithm from the corresponding period. The surface temperature composite map of the day of June 4th, 2008 showed the appearance of a positive thermal anomaly towards an area in the south of the Bousfer earthquake epicentre. This anomaly was intensified to a maximum build-up of thermal anomaly on June 5th, 2008 covering an approximate area around of 65,000 Km^2. The temperature rose to around 295–302ºK, about 5–6ºK higher than the surrounding area. After two main shocks occurred, of magnitudes 4.2 Mw (in 35.775N, 0.592W at 21:10 UTC) and 4.5 Mw (in 35.827N,

0.63W at 22:48 UTC) on 6 June 2008, the anomaly weakened. A less intense anomaly on the same night was probably a precursor to an earthquake of a magnitude of 2.9 Mw, which occurred at 23:33 (UTC). The anomaly disappeared in the afternoon of 7 June (Figure 3). Table 2 recapitulates details of June 6, 2008 Oran primary and aftershocks earthquakes even studied for pre-earthquake thermal anomaly.

Figure 4 Oran 6-6-2008 earthquake Mw 5.6 (EMC source), (a) geographic localisation and depth of the earthquake (b) historical seismicity from 1964 to 6-6-2008 in the north west of Algeria (the 'Oranie' region) (c) data reception at the EMSC from the network contributions to the database storage (d) regional moment torsors (see online version for colours)

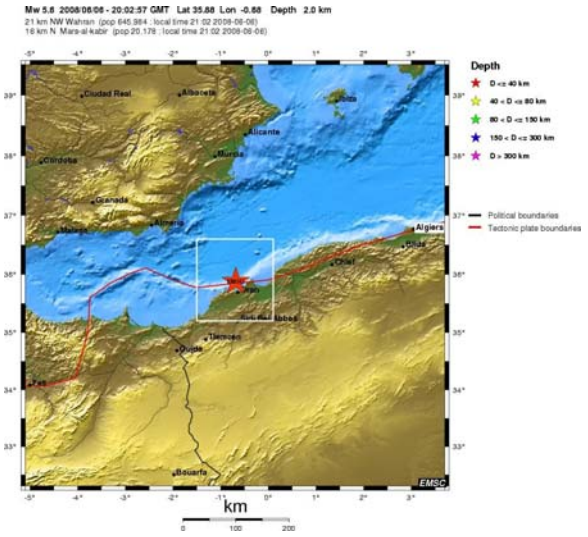

(a)

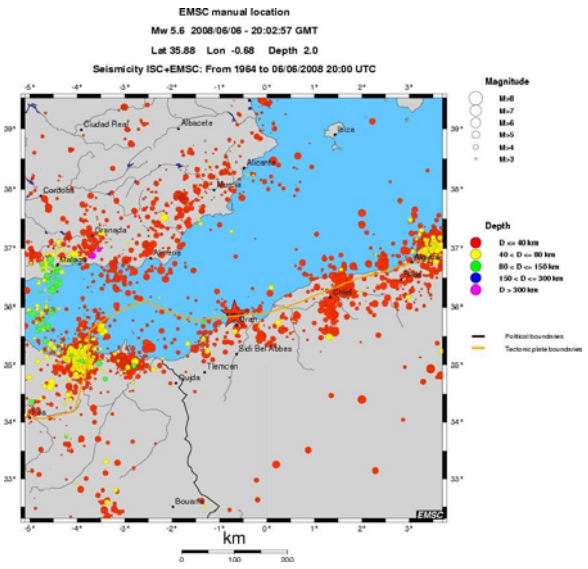

(b)

Figure 4 Oran 6-6-2008 earthquake Mw 5.6 (EMC source), (a) geographic localisation and depth of the earthquake (b) historical seismicity from 1964 to 6-6-2008 in the north west of Algeria (the 'Oranie' region) (c) data reception at the EMSC from the network contributions to the database storage (d) regional moment torsors (continued) (see online version for colours)

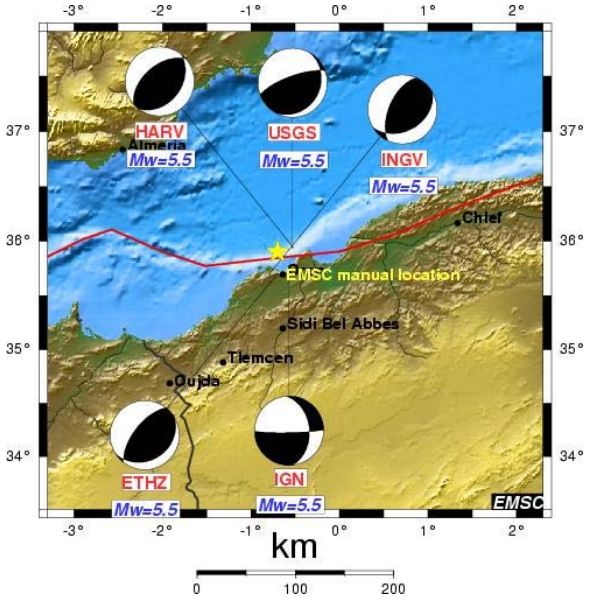

(c)

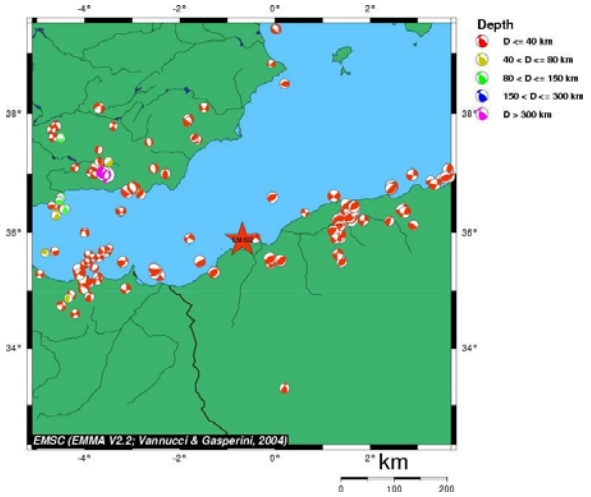

(d)

Figure 5 Time series composite SEVIRI raw IR3.9 channels acquired from 4 to 7 June 2008 at 12:00 UTC (before and after the earthquake) with the corresponding histogram (see online version for colours)

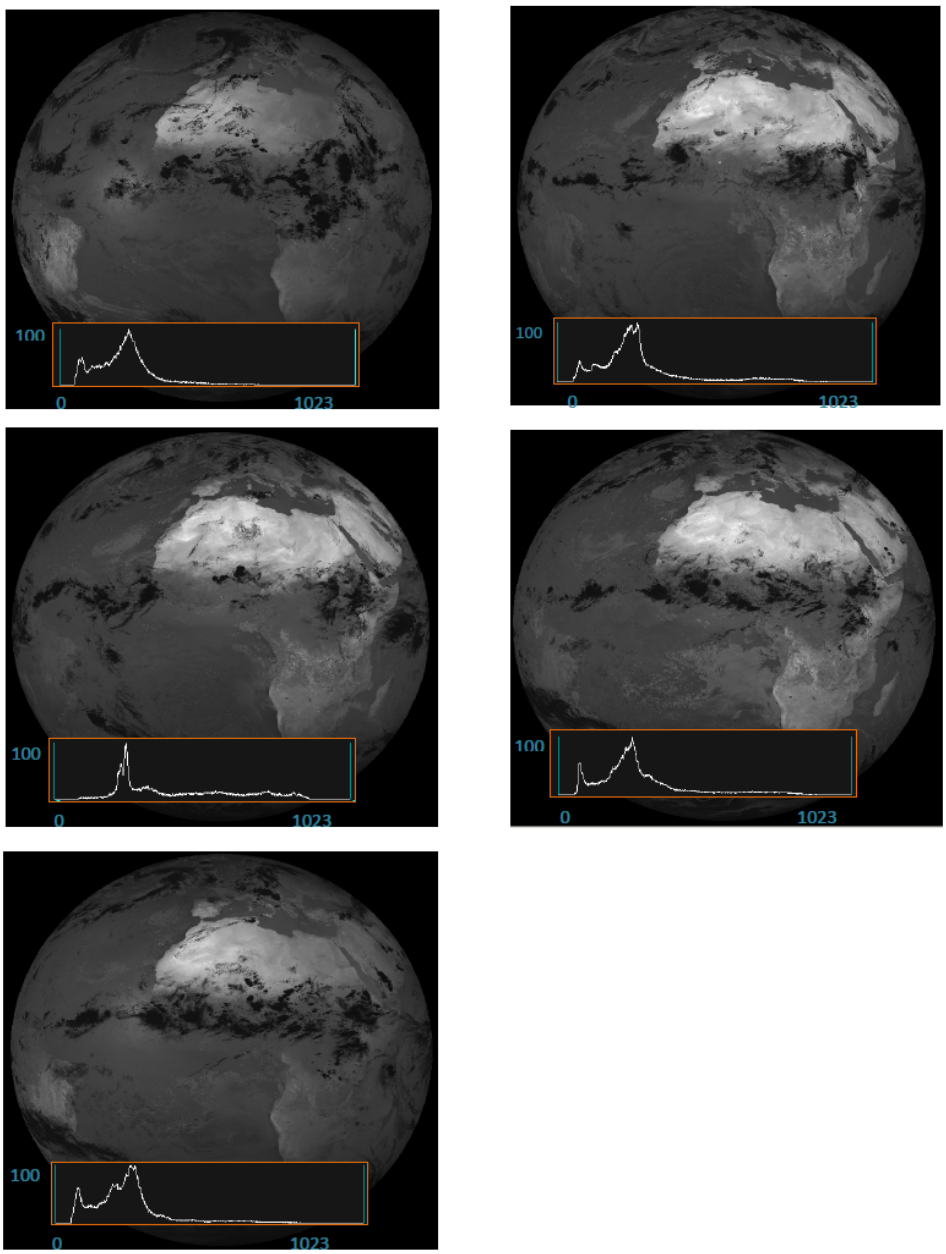

Figure 6 Time series composite surface temperature maps of Algeria before and after the earthquake (see online version for colours)

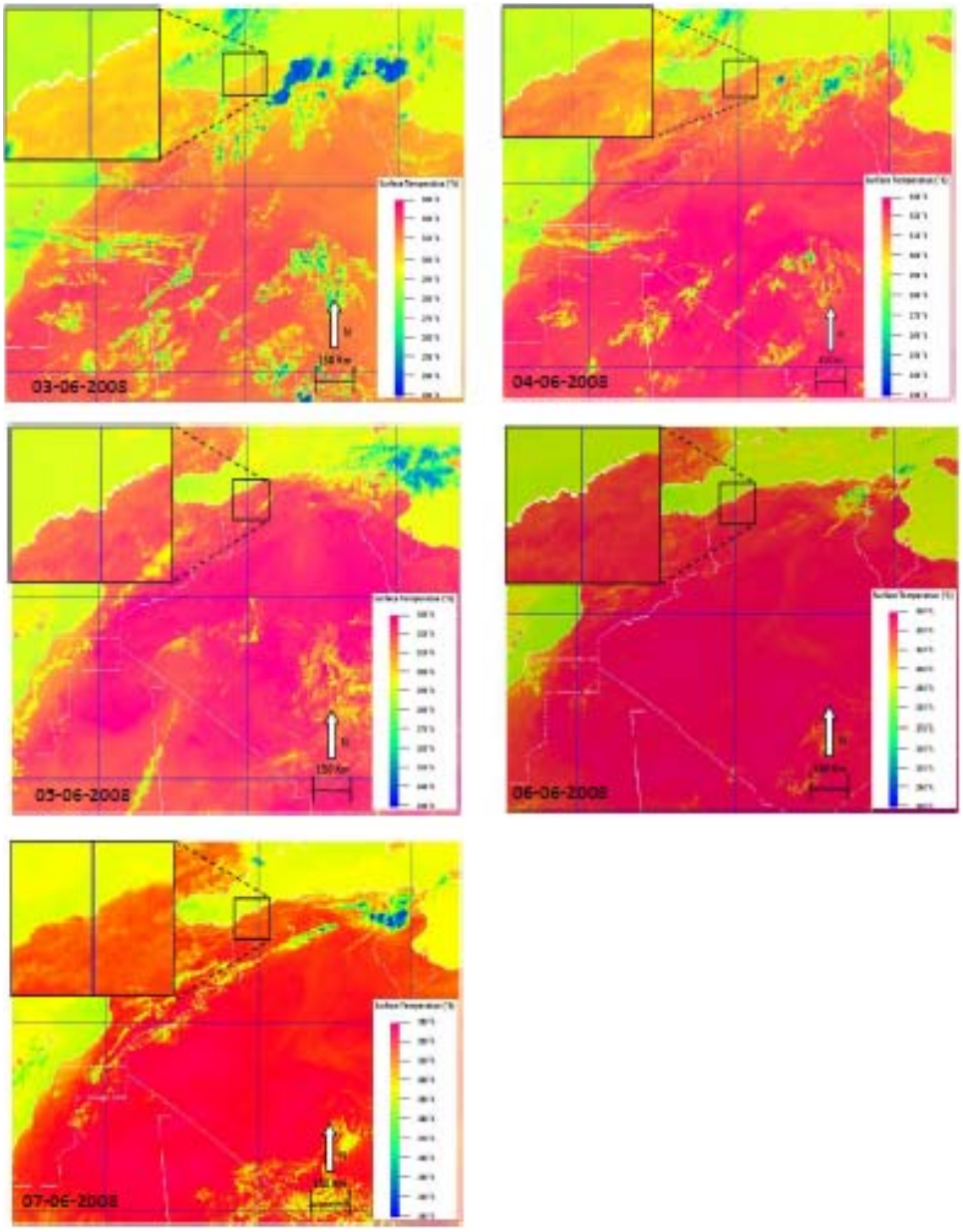

Note: The temperature was seen to be maximum on June 6, 2008 at 12:00 UTC.

To validate the AEPA algorithm, another event was covered in this research, the Blida earthquake (Ms = 4.6) occurred at 20:03 (UTC) on May 23rd, 2013, and it was detectable from 19 Km in SE of Larbra-Blida, the epicentre was at 36.44N, 3.31E. Three days later (on May 26, 2013 at 16:00:55 UTC), an earthquake (Ms = 5.0) occurred at 8 Km ESE of Bejaia-Algeria (36.736°N, 5.178°E) Depth: 10.0 Km, because of the masking of the

ground caused by the presence of clouds in Bejaia region from the 24th to the 27th of May 2013, we have limited this validation to Blida earthquake. Figure 7 presents a scenario covering this event illustrated from the EMSC.

Table 2 Details of June 6, 2008 Oran primary and *aftershocks* earthquakes studied for pre-earthquake thermal anomaly

Epicentre location	*Time (UTC)*	*Magnitude (Mw)/depth (Km)*	*Surface temperature (°K) on June 4, 2008*	*Surface temperature (°K) on June 5, 2008*	*Surface temperature (°K) on June 6, 2008*	*Range of temperature increase (°K)*
35.883N, 0.658W	20:02	*5.5/4*	302	303	307	5
35.775N, 0.592W	21:10	*4.2/0*	302	304	307	5
35.875N, 0.602W	22:26	*3.3/0*	301	302–303	304	3
35.827N, 0.63W	22:48	*4.5/0*	301–302	301–302	306–307	5 to 6
35.903N, 0.547W	23:33	*2.9/0*	302	302	306	4

Figure 8 shows time series composite SEVIRI raw IR3.9 channels acquired from the 4th to the 7th of June 2008 at 12:00 UTC (before and after the earthquake) with the corresponding histogram.

An outstanding characteristic of the earthquake precursor is a bursting increase in temperature of the TIR channel obtained from satellite imagery. Image from 23 May 2013 in Figure 9 shows the temperature field distribution of the northern of Algeria, in which a dark orange area can be seen very clearly around 36N, 3–4E. This is the anomalous area of temperature increase with an area of over 5,000 Km^2. The temperature in this area was 3°K to 5°K higher than that in the surrounding areas. The light blue and blue colour on the east side of this area shows the cumulus line formed by cold air entering the sea; in the meantime the temperature was increasing in the coastal region of Bejaia city. Many houses and buildings have been slightly damaged (cracks, etc.) and that 2 houses have been seriously damaged. Four persons are reported injured.

The proposed method can distinguish the temperatures anomalies detections from 2°K to 6°K, it is more sensitive than others method like proposed by Choudhury (2005) which significant thermal anomalies with a rise in temperature of about 5–10°K in the vicinity of the epicentres have been observed, on the other hand, SEVIRI sensor presents a rapid radiometer (temporal resolution 15 min) with a fixed field of view (embedded on MSG3 geostationary satellite), advanced very high resolution radiometer (AVHRR) embedded on NOAA polar satellite series presents a period of revisit around ten days (low temporal resolution), the geometric correction and geolocalisation operations of each image data are very complicated operations compared to SEVIRI images data.

AEPA algorithm is more accurate alternative to the GPS method (Freund et al., 2007). The last one relies on measurements of the slight deformation of the Earth's crust that occurs before an earthquake.

Figure 7 Blida 23-5-2013 earthquake Mw 4.6 (EMC source), (a) geographic localisation and depth of the earthquake in global plan (b) geographic localisation and depth of the earthquake in local plan (c) historical seismicity from 1964 to 23-5-2013 in the north of Algeria (d) regional moment torsors (see online version for colours)

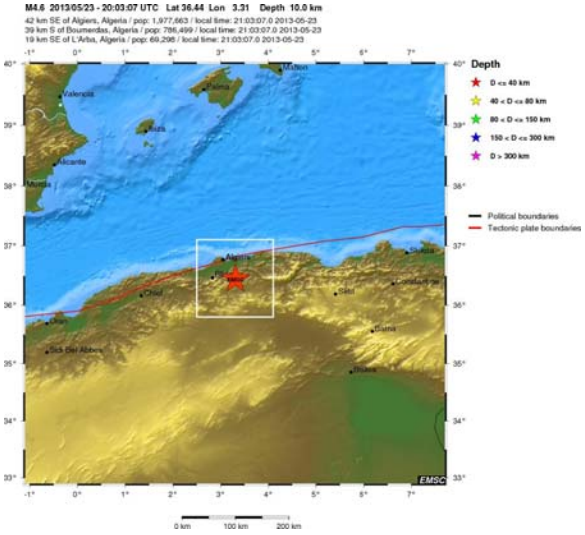

(a)

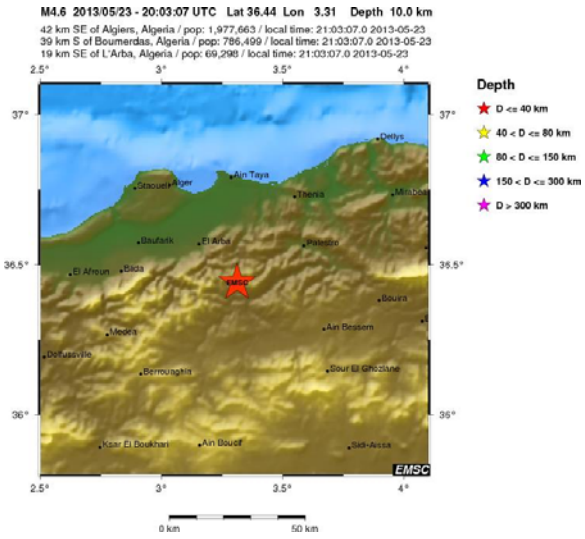

(b)

Figure 7 Blida 23-5-2013 earthquake Mw 4.6 (EMC source), (a) geographic localisation and depth of the earthquake in global plan (b) geographic localisation and depth of the earthquake in local plan (c) historical seismicity from 1964 to 23-5-2013 in the north of Algeria (d) regional moment torsors (continued) (see online version for colours)

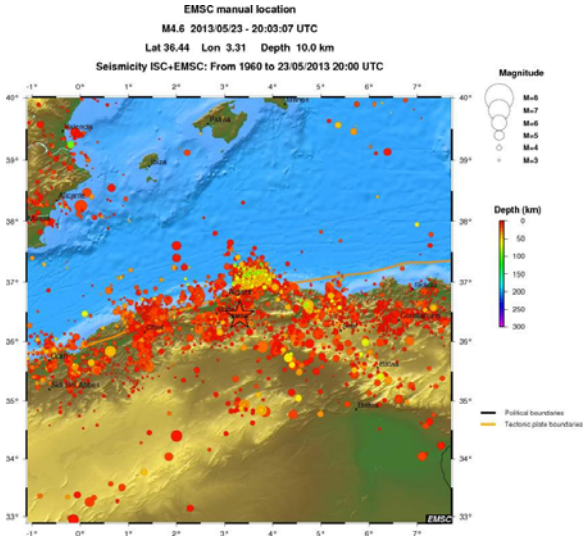

(c)

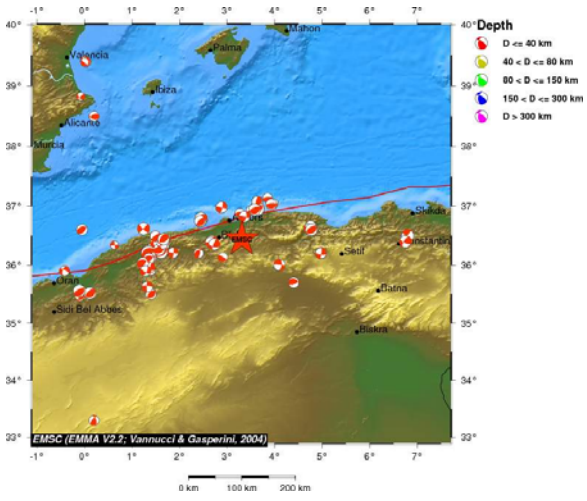

(d)

AEPA based on a global rapid soil surface temperature anomalies detection can be used to accomplish other future researches as done by Chmyrev et al. (2013). Chmyrev's work presented a proposal for coordinated experimental studies of lithosphere-atmosphere-ionosphere (LAI) coupling effects associated with seismic activity particularly as precursors to earthquakes. Chmyrev's proposed program would include the flight of two TwinSat co-orbiting satellites (TwinSat-1N and TwinSat-1M) that will make a range of measurements in the ionosphere and coordinated ground-based observations.

Figure 8 Time series composite SEVIRI raw IR3.9 channels acquired from 20 to 24 May 2013 at 12:00 UTC (before and after the earthquake) with the corresponding histogram (see online version for colours)

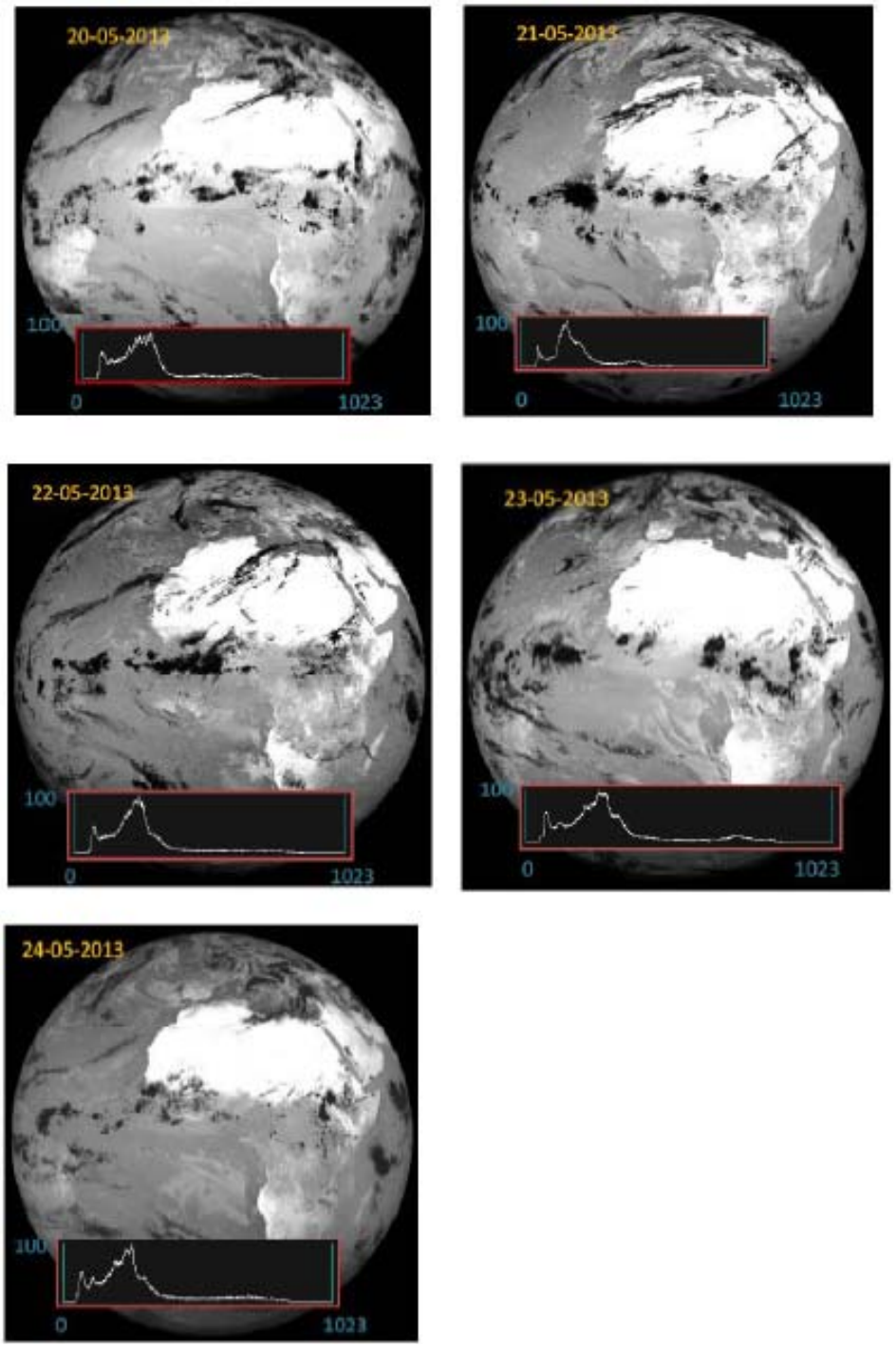

Figure 9 Time series composite surface temperature maps of North Algeria before and after the earthquake (see online version for colours)

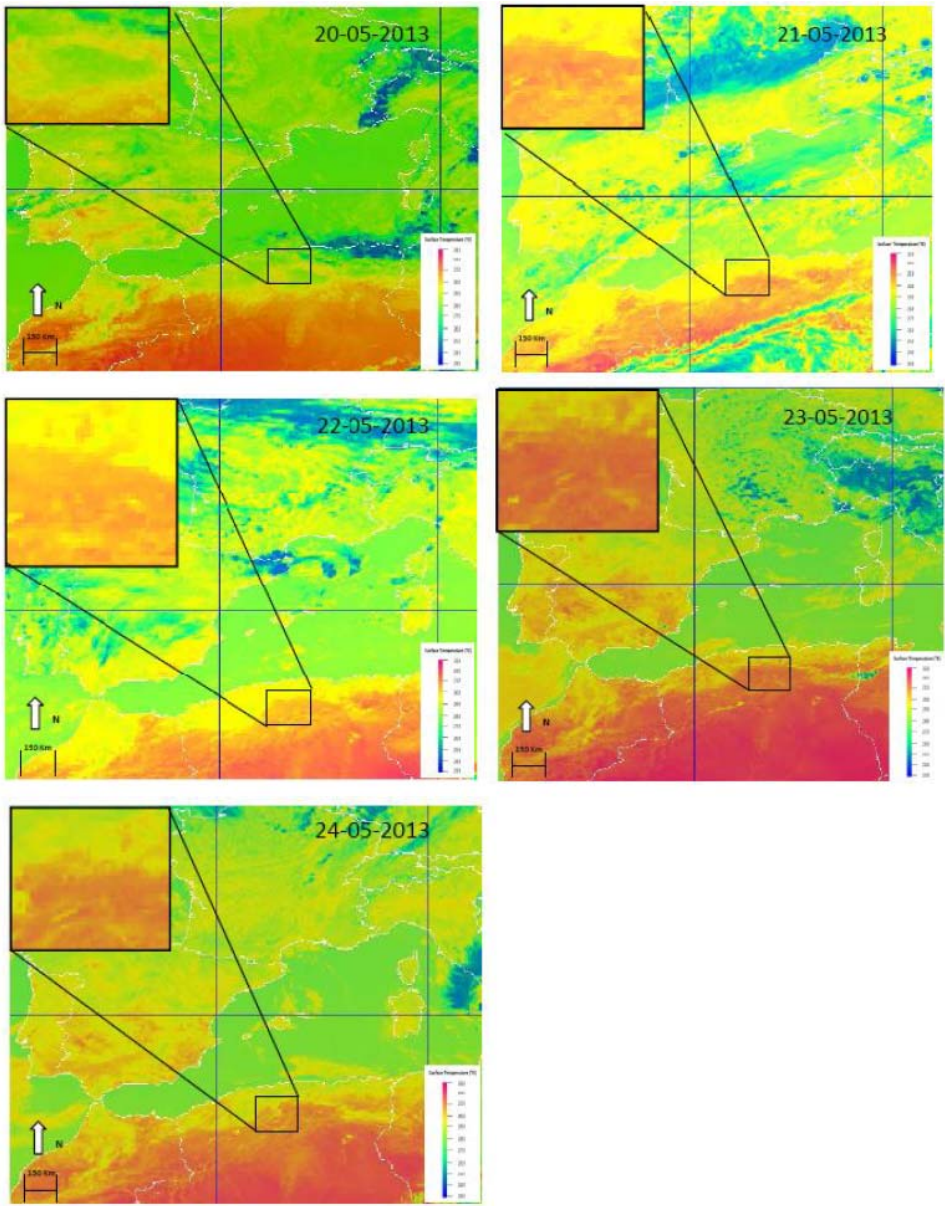

Note: The temperature was seen to be maximum on May 23, 2013 at 12:00 UTC.

4 Conclusions

The proposed AEPA method for earthquake prediction has been shown to provide timely information on earthquakes more accurately and economically than other proposed methods. From 2007 to the present time, an important earthquake was occurred in June 2008 in Oran city (North West of Algeria), with a magnitude around 5.5 Ms, the disaster resulted in the without any loss of lives, over 30 severe injuries and an estimated direct financial loss. As successfully demonstrated in the present study, the earthquakes in Oran (Algeria), was associated with the presence of pre-earthquake thermal anomalies. The anomalies appeared a few days to a few hours before the earthquakes. The increase in temperature ranges between 4°K to 6°K. These anomalies are seen to disappear after the earthquakes. The AEPA method is validated with other earthquake happened in Blida (north of Algeria), it offers an inexpensive and potentially more accurate alternative and sensitive than other methods of earthquake detection. Because of the wide coverage and ready availability of data from SEVIRI, many other areas of the world could potentially benefit from the technique within a short timescale and for very little investment. One potential drawback of the technique is the masking of the ground caused by the presence of clouds in some infrared imagery; experience has shown that this may be overcome by using the short wave infrared radiometers carried on meteorological satellites. Proposals are also currently being put forward to use the same satellite TIR data to study precursors of volcanic eruptions. The following perspectives proposed by this research work deserve careful attention and need to be solved:

- undetected clouds, sub-pixel clouds, temperature anomalous soil pixels under thin cirrus
- mixed water (river/lake/coast) and land scenes
- inhomogeneous land surfaces
- unknown land surface emissivities, in particular in IR3.9 channel
- dusk and dawn periods with rapidly changing IR3.9 channel values
- generalising the prediction to larger possible regions of the observed soil Earth
- proposing to develop an e-bulletin for each event within which users will access all seismological products and scientific documentation related to it.

References

Ahrens, C.D. and Henson, R. (2014) *Meteorology Today: An Introduction to Weather, Climate, and the Environment*, 11th ed., Cengage Learning, Boston, 656pp.

Bristor, C.L. (1975) *Central Processing and Analysis of Geostationary Satellite Data*, NOAA Technical Memorandom NESS 64, US Department of Commerce, National Oceanic and Atmospheric Administration, Washington, DC, 155pp.

Chmyrev, V., Smith, A., Kataria, D., Nesterov, B., Owen, C., Sammonds, P., Sorokin, V. and Vallianatos, F. (2013) 'Detection and monitoring of earthquake precursors: TwinSat, a Russia-UK satellite project', *Advances in Space Research*, Vol. 52, No. 6, pp.1135–1145.

Choudhury, S. (2005) *Development of Remote Sensing Based Geothermic Techniques in Earthquake Studies*, Unpublished PhD thesis, Department of Earth Sciences, Indian Institute of Technology Roorkee, Roorkee, India.

Curtis, A.B. and Edwards, L. (2004) *Zemmouri, Algeria, Mw6.8 Earthquake of May 21, 2003*, Technical Council of Lifeline Earthquake Engineering (TCLEE) Monographs, ASCE, Reston, VA, 120pp.

Freund, F., Takeuchi, A., Lau, B.W.S., Al-Manaseer, A., Fu, C.C., Byrant, N.A. and Ouzounov, D. (2007) 'Stimulated infrared emission from rocks: assesig a stress indicator', *eEarth*, Vol. 2, No. 1, pp.7–16.

Godey, S., Bossu, R. and Guilbert, J. (2013) 'Improving the Mediterranean seismicity picture thanks to international collaborations', *Physics and Chemistry of the Earth*, Vol. 63, No. 1, pp.3–11.

Godey, S., Bossu, R., Guilbert, J. and Mazet-Roux, G. (2006) 'The Euro-Mediterranean bulletin: a comprehensive seismological bulletin at regional scale', *Seismological Research Letters*, Vol. 77, No. 4, pp.460–474.

Hassini, A. and Belbachir, A.H. (2013) 'Hardware and software consideration to use near real time MSG-SEVIRI and NOAA-AVHRR images', *11th International Symposium on Programming and Systems (ISPS'2013)*, Algiers, Algeria, 22–24 April, pp.12–16.

Hassini, A. and Belbachir, A.H. (2014) 'Thermal method of remote sensing for prediction and monitoring earthquake', *Proceedings of the 1st IEEE International Conference on ICTs for Disaster Management (ICT-DM'2014)*, CERIST-Algeirs, 24–25 March, pp.89–92.

Hassini, A., Benabdelouahed, F., Benabadji, N. and Belbachir, A.H. (2009) 'Active fire monitoring with level 1.5 MSG satellite images', *American Journal of Applied Sciences*, Vol. 6, No. 1, pp.157–166.

Kerkmann, J. (2004) *Applications of Meteosat Second Genaration (MSG): Meteorological Use of the SEVIRI IR3.9 Channel*, EUMETSAT course [online] http://oiswww.eumetsat.org/IPPS/html/bin/guides/msg_rgb_convection.ppt (accessed 9 January 2015).

Ma, J., Chen, S., Hu, X., Liu, P. and Liu, L. (2010) 'Spatial-temporal variation of the land surface temperature field and present-day tectonic activity', *Geoscience Frontiers*, Vol. 1, No. 1, pp.57–67.

Platt, C.M.R. (1991) 'Remote sensing in hydrological and a grometeorological applications', *Proceedings of the Fifth UN/FAO/WMO/ESA Training Course*, CSIRO Office of Space Science & Applications (COSSA), COSSA Publication 026, Canberra, Australia, 236pp.

The European-Mediterranean Seismological Centre (EMSC) (2015) [online] http://www.emsc-csem.org (accessed 10 January 2015).

Tronin, A.A. (2010) 'Satellite remote sensing in seismology. A review', *Remote Sens*., Vol. 2, No. 1, pp.124–150.